Geomechanics and Engineering, *Vol. 23, No. 5 (2020) 481-491*
DOI: https://doi.org/10.12989/gae.2020.23.5.481

Estimation of lateral pile resistance incorporating soil arching in pile-stabilized slopes

C.R. Neeraj[a] and Sudheesh Thiyyakkandi*

Department of Civil Engineering, Indian Institute of Technology Palakkad, Kerala 678621, India

(Received July 24, 2020, Revised November 24, 2020, Accepted November 28, 2020)

Abstract. Piles installed in row(s) are used as an effective technique to improve the stability of soil slopes. The analysis of pile-stabilized slopes require a reliable prediction of lateral resistance offered by the piles. In this work, an analytical solution is developed to estimate the lateral resistance offered by the stabilizing piles in sand and $c-\phi$ soil slopes considering soil arching phenomenon. The soil arching in both horizontal direction (between the neighboring piles) and vertical direction (in the active wedge in front of the pile row) are studied and their effects are incorporated in the proposed model. The shape of soil arch is assumed to be circular and principal stress trajectories are defined separately for both modes of arching. Experimental and numerical studies found in literature were used to validate the proposed method. A detailed parametric analysis was performed to study the influence of pile diameter, center-to-center spacing, slope angle and angle of internal friction on the lateral pile resistance.

Keywords: pile-stabilized slopes; soil arching; lateral pile resistance; $c-\phi$ soil; slope angle

1. Introduction

The use of stabilizing piles in row(s) is one of the common operative techniques employed for slope stabilization and prevention of excessive soil movement (Ito and Matsui 1975, Hassiotis *et al.* 1997, Cai and Ugai 2000, Kourkoulis *et al.* 2011a, Lirer 2012, Liang *et al.* 2014, Ho 2015, Saseendran and Dodagoudar 2020). The existing analytical methods for analysis of pile-stabilized slope and computation of the pile resistance can be generally classified into two categories, i) displacement-based methods, and ii) pressure-based methods (Jeong *et al.* 2003, Ho 2015). The lateral force predicted by displacement-based methods (Lee *et al.* 1995, Jeong *et al.* 2003, Ashour and Ardalan 2012, Galli and Di Prisco 2013) is the mobilized pile resistance which is a function of soil and pile deformation; while the pressure-based methods (Ito *et al.* 1981, Hassiotis *et al.* 1997, Won *et al.* 2005, He *et al.* 2015a) pertain to the ultimate state and provide soil-pile resistance at the limiting condition.

The displacement-based methods incorporate the inter-dependency of mobilized lateral force and pile deflection. Poulos (1995) reported a simplified boundary element method to estimate the lateral pressure on a single pile in response to lateral soil movement. Lee *et al.* (1995) introduced an uncoupled approach by utilizing Poulos (1995)'s method for estimating the pile resistance. Ausilio *et al.* (2001) presented a kinematic approach of limit analysis, which does not take into account the pile-spacing and arching between adjacent piles. Jeong *et al.* (2003) presented an uncoupled analysis for weathered pile-reinforced slopes using a load transfer approach for the pile resistance. Ashour and Ardalan (2012) proposed an approach by adopting the "flow mode" mechanism developed by Poulos (1995) to the strain wedge model (Norris 1986) for the lateral response of the pile, assuming a passive wedge in front of the piles. Though the displacement-based methods are generally considered to be better than the pressure-based methods, a major issue with them is the need of accurate measurement of lateral soil movement as input parameter, which is very difficult to obtain in the field (Liang and Zeng 2002, Won *et al.* 2005).

The pressure-based methods for estimating the ultimate lateral force on stabilizing piles stem from classical earth pressure theories. A rupture condition based calculation method by adopting estimated yield values for the pile-soil interaction was introduced by De Beer and Wallays (1970). Broms (1964)'s method for ultimate lateral load capacity of vertical pile in cohesive soil was used by Viggiani (1981) to estimate the lateral load on the stabilizing piles, which do not account for the effect of pile spacing. Ito and Matsui (1975) proposed a method to estimate the lateral forces on the stabilizing piles based on the theory of plastic deformation. The theory considers the squeezing of soil between two piles and assumes that the soil become plastic only in a narrow zone adjacent to the piles and Rankine's active earth pressure acts along the central plane of the pile row. Past research have reported that the soil adjacent to the piles is subjected to horizontal soil arching which changes the orientation of principal planes (Bosscher and Gray 1986, Adachi *et al.* 1989, Liang and Zeng 2002, Durrani *et al.* 2006, Ellis *et al.* 2010). This horizontal arching effect is

*Corresponding author, Assistant Professor, Ph.D.
E-mail: sudheesh@iitpkd.ac.in
[a]Research Scholar
E-mail: cr.neeraj@gmail.com

ISSN: 2005-307X (Print), 2092-6219 (Online)

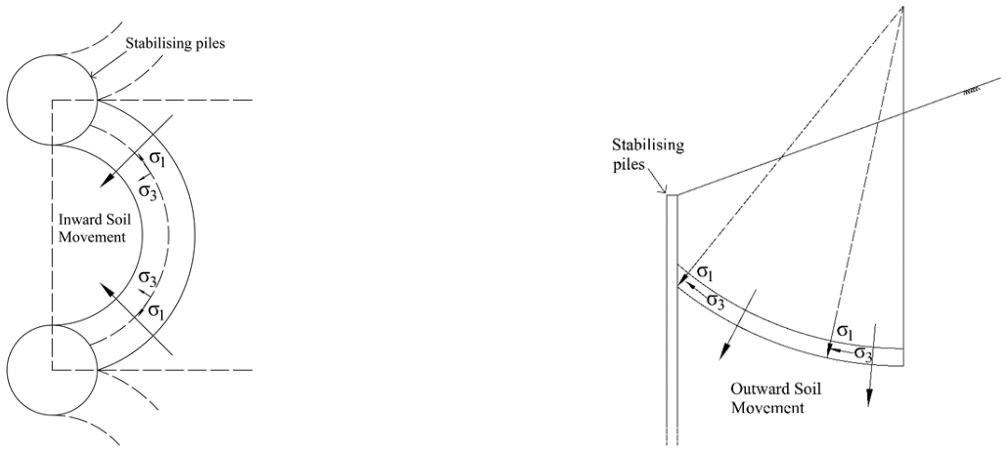

(a) (b)

Fig. 1 Schematic representation of (a) horizontal arching (Mode 1) and (b) vertical arching (Mode 2) in the pile-stabilized slope

due to the differential lateral deformation of soil mass in front of the pile row. However, Ito and Matsui (1975)'s theory ignore the rotation of principal stresses in the plastic zone and approximates normal stress on shearing plane as major principal stress and the direction of minor principal stress to be normal to the row of the piles throughout the stretch of plastic zone. Therefore, the method has to be used cautiously in cohesionless soils (Bosscher and Gray 1986). Several pressure-based methods were proposed since then to determine the lateral force on the piles and many of them are either based on or derived from the method developed by Ito and Matsui (1975) (Harrop-Williams 1989, Won *et al.* 2005, Song *et al.* 2012, He *et al.* 2015a, b, Li and Wei 2018, Deng and Yang 2019). More recently, Di Laora *et al.* (2017) have extended Viggiani's (1981) solutions for ultimate load on the stabilizing piles for free- and fixed-head pile with infinite and finite flexural capacity in drained and undrained conditions. However, the solutions apparently do not consider the influence of the pile spacing and soil arching. Ito and Matsui (1975)'s classic theory was extended for the case of unsaturated soil slopes incorporating the effect of suction by Deng and Yang (2019); however, the effect of soil arching is not considered.

Besides horizontal arching, the soil in front of the pile row is subjected to vertical arching as it deforms vertically and therefore, the lateral earth pressure distribution in soil between the adjacent piles will no longer be linear (He *et al.* 2015a, b, Lee *et al.* 2016). Several studies in past have proposed methods to obtain the non-linear active earth pressure behind a retaining wall incorporating the effect of vertical soil arching (Paik and Salgado 2003, Li and Wang 2014, Rao *et al.* 2016). He *et al.* (2015a) adopted Paik and Salgado (2003)'s approach for estimating non-linear active earth pressure along the central plane of the pile row installed in sandy slopes. Later, He *et al.* (2015b) have extended this to $c-\phi$ soil with horizontal ground surface (slope angle = 0). However, their equations are not applicable for a general case of $c-\phi$ soil with slope angle greater than zero. In addition, both He *et al.* (2015a, b) adopted Ito and Matsui's (1975) formulation to estimate the lateral forces on the stabilizing piles and therefore, the limitations in the assumption made by Ito and Matsui (1975) is inherited to their work as well (He *et al.* 2015a).

This work aims to develop an analytical model based on the concept of soil arching for determining the resistance offered by the row of piles installed in sand and $c-\phi$ soil slopes incorporating the influence of the pile diameter, spacing, slope parameters and soil properties. The proposed pressure-based model considers soil arching in the horizontal and vertical direction separately. The method is validated for both sand and $c-\phi$ soil by comparing with the field measurements and numerical studies found in literature. In addition, the effects of various parameters such as the pile diameter, center to-center spacing, slope angle, and angle of internal friction are studied through a detailed parametric analysis.

2. Soil arching in pile-stabilized slope

Based on the orientation of principal planes, soil arching can be categorized into two modes (Wang *et al.* 2017, Khosravi *et al.* 2018). In the first mode of arching, the soil movement is radially inward and the arch is formed along the trajectory of major principal stress. This is observed to happen in the case of deep tunnels, piled-embankments, undercut slopes, etc. (Hewlett and Randolph 1988, Wang *et al.* 2017). On the other hand, in the second mode, the soil deforms radially outward and the arch is formed depicting the trajectory of minor principal stress, for example, silo filled with bulk solids, pipeline ditches, retaining walls, hoppers, etc. (Paik and Salgado 2003, Wang *et al.* 2017, Jaouhar *et al.* 2018). In case of pile-stabilized slopes, the horizontal arching is the first mode and the second mode of arching occurs in the vertical direction. Fig. 1 shows a schematic representation of horizontal and vertical arching in the pile-stabilized slopes. As the arch action is initiated by rotation of principal stresses, the shape of arching zone is defined in terms of principal stress directions (Handy 1985, Bosscher and Gray 1986, Harrop-Williams 1989, Paik and Salgado 2003, He *et al.* 2015a). Due to the complex differences mentioned earlier, horizontal arching and vertical arching need to be analyzed separately.

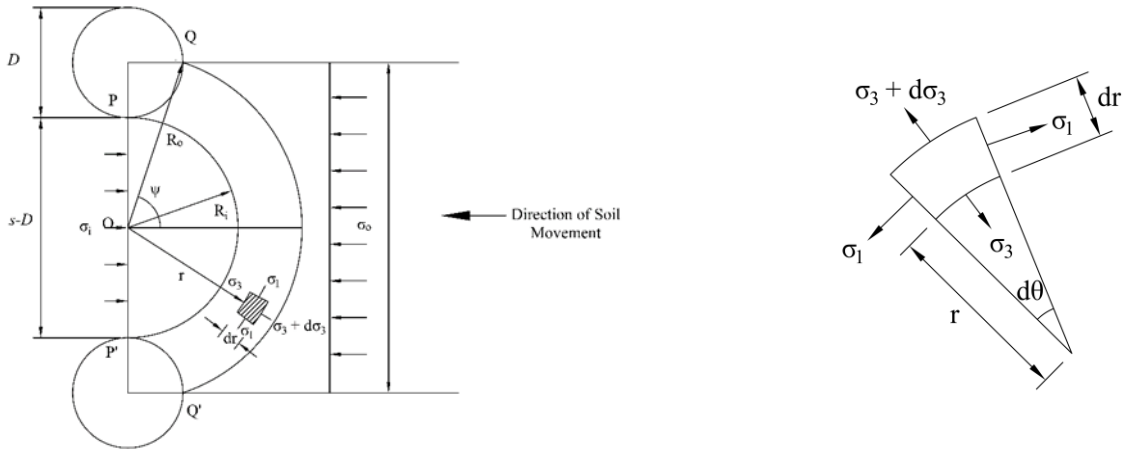

(a) (b)

Fig. 2 (a) Plan view of the arching zone under lateral loading and (b) a differential element of thickness dr at radius, r

Analysis of arching in a piled-embankment (1st mode arching) revealed that, in order to satisfy static equilibrium, the soil arch attains semi-circular shape of uniform thickness, spanning over adjacent supports without overlap (Hewlett and Randolph 1988). Several other shapes of arches such as triangular and parabolic in two-dimension, and hemispherical, domal and corbelled in three-dimension have also been observed in past researches (Kellogg and Quinlan 1987, Adachi *et al.* 1989, Chen and Martin 2002). Handy (1985) approximated the shape of vertical soil arch behind the retaining wall (2nd mode arching) as catenary, the shape attained by a freely hanging chain, assuming soil to be homogeneous and isotropic with uniform weight throughout the zone. Harrop-Williams (1989) studied the arching process behind a retaining wall and inferred that the shape of arch can be reasonably assumed as circular. Paik and Salgado (2003) assumed a circular trajectory for minor principal stress in the case of vertical arching behind the retaining wall, which was adopted by He *et al.* (2015a, b) for the case of pile-stabilized slopes. A circular arch along the trajectory of the minor principal stress was assumed by Jaouhar *et al.* (2018) as well in their analytical model to estimate the stresses in vertical backfilled stopes. Previous studies have shown that the horizontal arching between adjacent stabilizing piles nearly follows a circular trajectory (Liang and Zeng 2002, Ardalan and Ashour 2013, Liang *et al.* 2014, He *et al.* 2015a). Therefore, in the present analysis, soil is assumed to arch along a semi-circle as shown in Fig. 1. Similarly, in case of vertical arch, the shape was adopted from Paik and Salgado (2003) and the equations for non-linear lateral pressure were re-derived as explained below.

3. Analytical model

The formulation of the analytical model for ultimate lateral resistance offered by the piles is based on the following assumptions. The deformation of sliding soil mass is assumed to be larger than the lateral deflection of the stabilizing piles; in essence, the present analytical method considers the "flow-mode of failure" as defined by Poulos (1995). The soil is assumed to be plastic in the arching zone and Mohr-Coulomb yield criterion is applied (Moradi and Abbasnejad 2015). In the case of horizontal arching, the soil mass is assumed to be in plane-strain condition as assumed by Ito and Matsui (1975). When the sliding of unstable soil layer occurs, the soil pressure from the upslope will partially get transmitted to the downslope through the soil in between the piles, depending on the spacing. It is assumed here that an active state of plastic equilibrium is reached at the interface of downslope and upslope soil masses between the neighboring piles due to the soil deformation as adopted in the previous studies (Ito and Matsui 1975, Viggiani 1981, Hassiotis *et al.* 1997, Won *et al.* 2005, He *et al.* 2015a, Deng and Yang 2019). Paik and Salgado (2003)'s approach for incorporating vertical arching within the active wedge is adopted to determine lateral stress along this interface (central plane of the pile row) as explained in subsequent section.

Piles of diameter D is placed in a row at a centre-to-centre spacing of s, such that the spacing to diameter ratio, $s/D = n > 1$. Fig. 2(a) represents the arching zone assumed in the horizontal direction. It is a semi-circular arch centered in the middle of adjacent piles. In the arching zone, $PQQ'P'$, the major principal stress acts tangentially and the minor principal stress is along the radial direction. The outer and inner radii of arching zone are R_o and R_i, respectively. The direction of loading is as shown in Fig. 2. To obtain the relationship between the stresses on outer and inner surface of the arching zone, a differential element of thickness dr is considered at radius, r (Fig. 2(b)). Both stress equilibrium equation (Eq. (1)) and Mohr-Coulomb yield criterion (Eq. (2)) will be applicable in the arching zone as it is assumed to be in plastic state.

$$\frac{\sigma_1 - \sigma_3}{r} - \frac{d\sigma_3}{dr} = 0 \tag{1}$$

$$\sigma_1 = N\sigma_3 + 2c\sqrt{N} \tag{2}$$

where, $N = \tan^2 45 + \phi/2$.

Combining Eq. (1) and Eq. (2) and integrating yields an expression for σ_3 as given by Eq. (3),

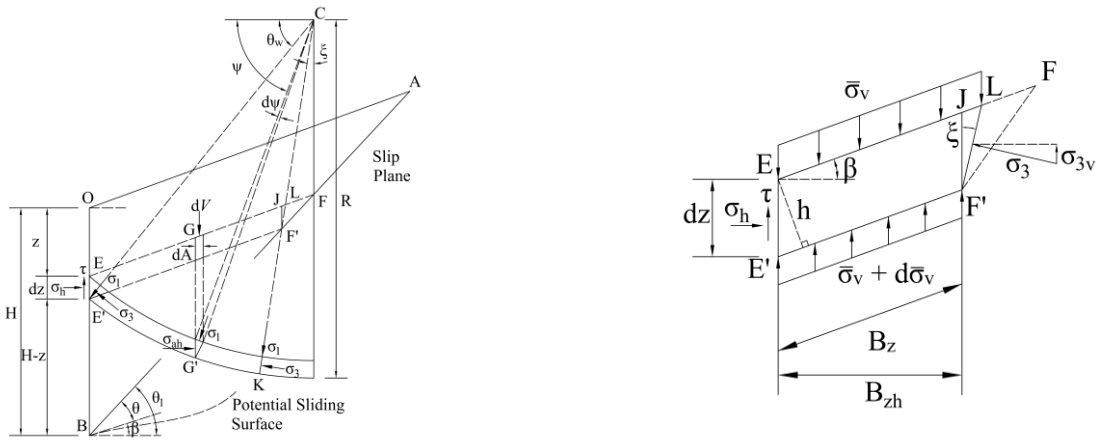

(a) (b)

Fig. 3 Stress state (a) of vertical arching zone in front of the pile row and (b) on differential element of height dz at E

$$\sigma_3 = \frac{(Ar)^{N-1} - 2c\sqrt{N}}{N-1} \tag{3}$$

The constant A can be obtained by applying boundary conditions (when $r = R_i;\ \sigma_3 = \sigma_i$) as,

$$A = \frac{\left[\sigma_1(N-1) + 2c\sqrt{N}\right]^{\frac{1}{N-1}}}{R_i} \tag{4}$$

Now, the radial stress at the outer boundary of arching zone can be obtained by substituting $r = R_o,\ \sigma_3 = \sigma_o$ in Eq. (3)

$$\sigma_o = \sigma_i \left(\frac{R_o}{R_i}\right)^{N-1} + \frac{2c\sqrt{N}}{N-1}\left[\left(\frac{R_o}{R_i}\right)^{N-1} - 1\right] \tag{5}$$

Eq. (5) gives the relationship between the stresses at outer and inner surfaces of the arch. The average stress on a plane before arching and after arching are approximated as σ_o and σ_i, respectively. Therefore, the lateral resistance from the pile at a given depth can be expressed as

$$P = \sigma_o(s) - \sigma_i(s - D) \tag{6}$$

Using Eq. (5) and substituting, $R_o = \sqrt{\left(\frac{D}{2}\right)^2 + \left(\frac{s}{2}\right)^2}$, $R_i = \frac{s-D}{2}$, and $n = \frac{s}{D}$, the expression for lateral resistance per unit length of the pile can be simplified as,

$$P = \sigma_i(\Lambda + 1)D + \frac{2c\sqrt{N}}{N-1}\Lambda D \tag{7}$$

where, $\Lambda = \left[\left(\frac{\sqrt{n^2+1}}{n-1}\right)^{N-1} - 1\right] n$

The coefficient Λ, coined as spacing coefficient, depends on ratio of centre-to-centre spacing to the pile diameter (n) and angle of internal friction (ϕ) of soil. It is evident from Eq. (7) that the first term is a function of soil stress (σ_i) along the central plane of the pile row and the second term depends on geometric and soil properties only.

As mentioned earlier, soil stress (σ_i) along the central plane will vary non-linearly with depth due to vertical arching of soil. In this study, an expression for active earth pressure considering the vertical soil arching for a general case of $c - \phi$ soil and sloped backfill is formulated as presented below. Fig. 3 shows the stress state of the vertical arching zone in front of the central line of the pile row. The slip plane of active wedge is assumed at an angle θ with respect to the ground surface (He *et al.* 2015a). A differential element $EFF'E'$ of thickness dz at depth z, is assumed to take a circular shape after vertical arching due to shear force developed along vertical plane OB (which lies along plane PP' in Fig. 2).

Considering the force equilibrium of a small triangle element at point E on OB, the lateral stress can be calculated using principles of Mohr circle as

$$\sigma_h = \sigma_1 \cos^2\theta_w + \sigma_3 \sin^2\theta_w \tag{8}$$

where, $\theta_w = \tan^2 45 + \phi/2$.

Similarly, the lateral stress at an arbitrary element at G which is shifted to point G' after arching is given by

$$\sigma_{ah} = \sigma_1 \cos^2\psi + \sigma_3 \sin^2\psi \tag{9}$$

where ψ is the inclination of normal to the arc at the arbitrary point G' to the horizontal.

Substituting the principal stress relation for active state, $\sigma_3 = \sigma_1/N - 2c/\sqrt{N}$, in Eq. (9) gives,

$$\sigma_{ah} = \sigma_1[\cos^2\psi + \frac{\sin^2\psi}{N}] - \frac{2c}{\sqrt{N}}\sin^2\psi \tag{10}$$

From the properties of origin of planes, $\sigma_1 + \sigma_3 = \sigma_v + \sigma_{ah}$, where, σ_v is the vertical stress at the surface of differential element. Substituting for σ_{ah} in Eq. (10) yields,

$$\sigma_v = \sigma_1[\sin^2\psi + \frac{\cos^2\psi}{N}] - \frac{2c}{\sqrt{N}}\cos^2\psi \tag{11}$$

Due to the effect of arching, as can be seen from Eq. (11), σ_v varies with the ψ which ranges from θ_w to $\pi/2$. Therefore, average vertical stress $\bar{\sigma}_v$ along the differential element $EFF'E'$ can be estimated as

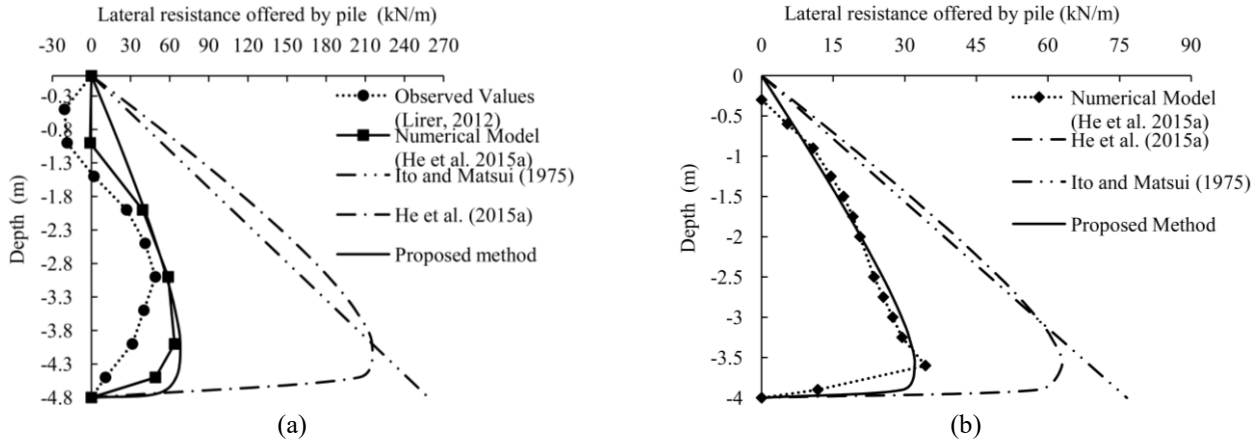

Fig. 4 Comparison of proposed method with (a) experimental studies of Lirer (2012) and (b) numerical model of He *et al.* (2015a)

$$\bar{\sigma}_v = \frac{1}{B_{zh}} \int_{\theta_w}^{\frac{\pi}{2}} \sigma_v dA \tag{12}$$

From geometry (Fig. 3), $dA = Rd\psi \sin\psi$; and the projected horizontal length of $EFF'E'$, $B_{zh} = R\frac{\cos(\theta_w+\xi)\cos\beta}{\cos(\beta+\xi)}$. Substituting these and Eq. (11) in Eq. (12) and rearranging yields,

$$\sigma_1 = \frac{\bar{\sigma}_v\left[\frac{\cos(\theta_w+\xi)\cos\beta}{\cos(\beta+\xi)}\right] + \frac{2c}{3\sqrt{N}}\cos^3\theta_w}{\cos\theta_w\left[1-\frac{N-1}{3N}\cos^2\theta_w\right]} \tag{13}$$

Substituting for σ_1 in Eq. 8 and writing σ_3 in terms of σ_1, we get

$$\sigma_h = K_{an}\bar{\sigma}_v + T \tag{14}$$

where,

$$K_{an} = \frac{\cos(\theta_w+\xi)\cos\beta}{\cos(\beta+\xi)}\left[\frac{3(N\cos^2\theta_w+\sin^2\theta_w)}{3N-(N-1)\cos^2\theta_w}\right]$$

$$T = \frac{2c}{\sqrt{N}}\left[\frac{\cos^2\theta_w(3(N\cos^2\theta_w+\sin^2\theta_w))}{3N-(N-1)\cos^2\theta_w} - \sin^2\theta_w\right]$$

The lateral force distribution on plane OB can be easily calculated using Eq. (14) if the vertical average stress $\bar{\sigma}_v$ is known. The presence of vertical arching necessitates an intricate analysis of differential element $EFF'E'$ (Fig. 3) to formulate an expression for $\bar{\sigma}_v$, as given below (derivation of Eq. (15) is presented in Appendix A).

$$\bar{\sigma}_v = \frac{\gamma\cos\beta\, H}{1-C_1}\left[\left(1-\frac{z}{H}\right)^{C_1} - \left(1-\frac{z}{H}\right)\right] + \frac{C_2}{C_1}\left[\left(1-\frac{z}{H}\right)^{C_1} - 1\right] \tag{15}$$

where,

$$C_1 = (K_{an}\tan\phi - K_{an}\tan\beta + m)\frac{\sin\theta}{\cos\theta_1};$$
$$m = \frac{K_{an}}{N\cos^2\theta+\sin^2\theta}\frac{\sin\xi\cos\beta}{\cos(\xi+\beta)} \tag{16}$$

$$C_2 = (T\tan\phi - K_{an}\tan\beta + m)\frac{\sin\theta}{\cos\theta_1};$$
$$t = c + \left(\frac{T+2c\sin^2\theta/\sqrt{N}}{N\cos^2\theta+\sin^2\theta}\right)\frac{\sin\xi\cos\beta}{\cos(\xi+\beta)} \tag{17}$$

It can be observed that Eq. (15) reduces to He *et al.* (2015b)'s equation when the slope angle, $\beta = 0$. Similarly, it reduces to He *et al.* (2015a)'s equation when soil is cohesionless. Therefore, it can be said that equations proposed by He *et al.* (2015a, b) are specific cases of Eq. (15). The non-linear vertical stress incorporating the effect of soil arching is used to calculate the lateral earth pressure distribution along the central line of the pile row (PP' in Fig. 2). That is, σ_h in Eq. (14) is assumed to act on the inner arch, giving the expression for σ_i in Eq. (7). The resultant lateral resistance from the pile can be expressed as (details of derivation of Eq. (18) is given in Appendix B),

$$P_r = D(\Lambda+1)K_{an}\left[\frac{\gamma\cos\beta\ H^2}{1-C_1}\left(\frac{1}{1+C_1}-\frac{1}{2}\right) + \frac{C_2H}{C_1}\left(\frac{1}{1+C_1}-1\right)\right] + TD(\Lambda+1)H + \frac{2c\sqrt{N}\ \Lambda DH}{N-1} \tag{18}$$

4. Model validation

The proposed theoretical model was validated for sand and $c-\phi$ soil conditions by comparing with results from the experimental and numerical studies available in literature. A brief description of each study and comparison of the results are presented below. The relevant material and geometric parameters of all the studies are summarized in Table 1.

For the model validation in sandy soils, the experimental study conducted by Lirer (2012) and the numerical analysis reported by He *et al.* (2015a) were used. Lirer (2012) conducted a well-instrumented field monitoring of stabilizing piles installed in an active mudslide in the Basento Valley, Southern Italy, to quantify

Table 1 Material and geometric parameters used for validation

Case	γ (kN/m^3)	c (kPa)	ϕ (^{o})	D (m)	n	β (^{o})
Basento Valley (Lirer 2012)	19.0	0	28.0	0.4	2.25	11.0
Numerical analysis (He *et al*. 2015a)	19.0	0	32.0	0.4	7.50	18.5
5# pile in Shabei I slope (Li and Wei 2018)	19.1	19.6	10.5	2.0	2.00	15-20

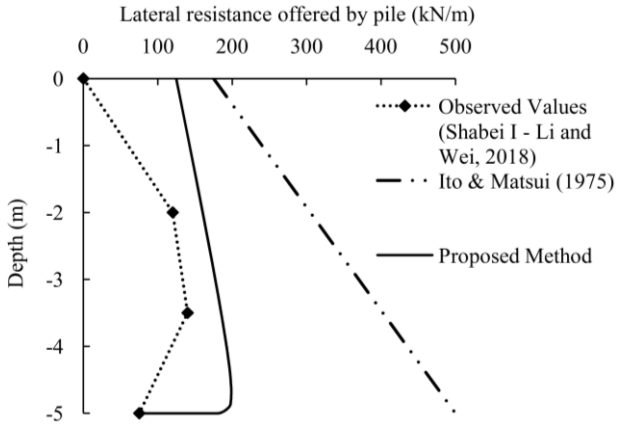

Fig. 5 Comparison of observed values and theoretical value of lateral load on pile at Shabei I slope (Li and Wei 2018)

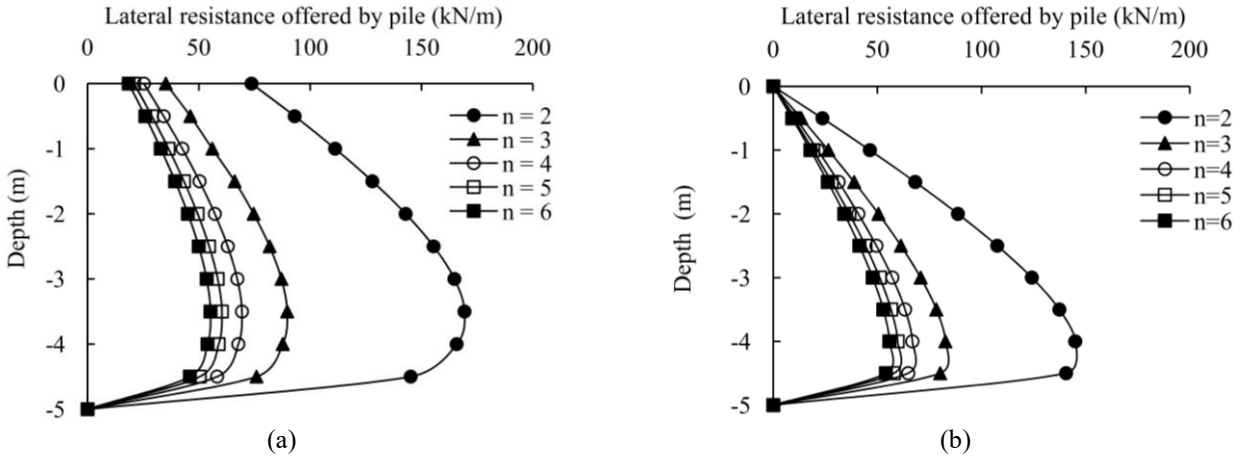

Fig. 6 Lateral resistance from the pile for different values of n for (a) $c-\phi$ soil and (b) Sandy soil (c = 0)

the shear force and bending moment distribution within the piles as well as to investigate the influence of row of piles on the mudslide displacement field. He *et al.* (2015a) had first validated their numerical model using the experimental work of Lirer (2012) as presented in Fig. 4(a). The numerical analysis results shown in Fig. 4(b) was with another set of soil parameters and a different slope angle (Table 1). Fig. 4 compares the predicted lateral pressure distribution on the pile using the proposed model with the experimental and numerical results. The predictions using the theoretical methods proposed by Ito and Matsui (1975) and He *et al.* (2015a) are also included in the figure. It is evident from the figure that the predictions using the proposed theoretical method are in good agreement with the experimental and numerical results. The observed results of Lirer (2012) suggest an "intermediate mode of failure (Poulos 1995)" and He *et al.* (2015a)' s numerical model developed using a finite difference program captures this actual mode of failure. However, the analytical methods developed by Ito and Matsui (1975), He *et al.* (2015a) and the proposed method are based on the assumptions of "flow mode of failure" (Poulos 1995) and therefore, the discrepancy in the predicted values at the shallow depths (Fig. 4(a)) may be attributed to this fact.

The validity of the model in typical $c-\phi$ soil was verified by applying the case study of Shabei I slope on the north of Hongfeng Station on Cheng-Kun Railway, China, reported by Li and Wei (2018). The slope is 50 m wide and spans for 100 m. The sliding layer was around 5-8 m deep. The soil is composed of pelitic siltstone and silty mudstone. Vibrating wire soil pressure cells were embedded at 1 m interval to monitor the earth pressure on 5# pile. Lateral pressure distribution for this case was predicted using the material and geometric parameters given in Table 1. The proposed method predicted the pressure distribution moderately well as can be seen from Fig. 5.

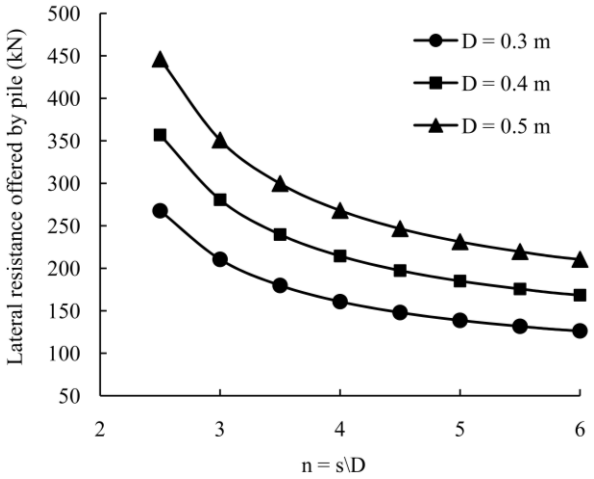

Fig. 7 Resultant lateral pile resistance for various s/D ratio

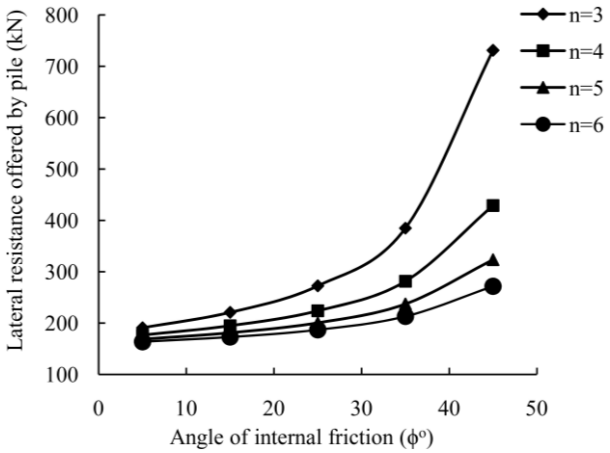

Fig. 8 Variation of lateral pile resistance with angle of internal friction

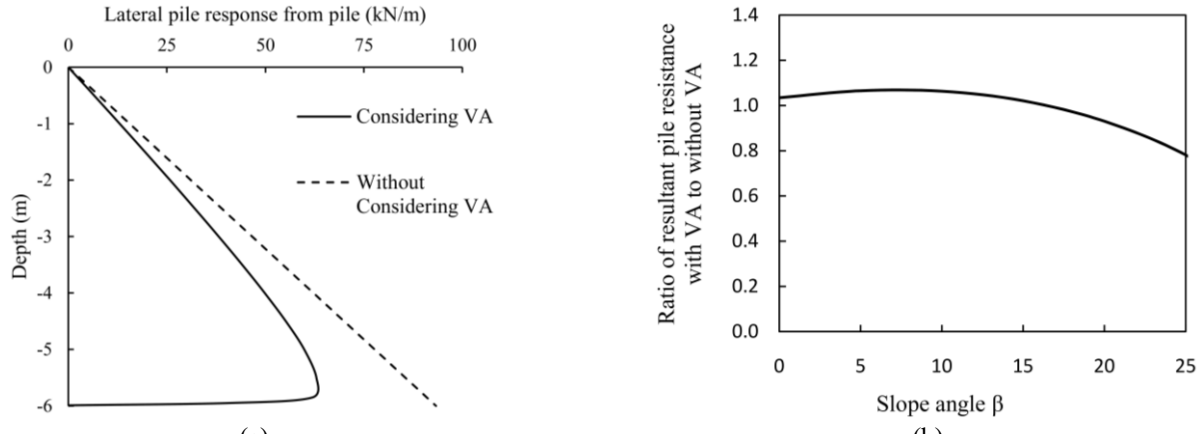

(a) (b)

Fig. 9 (a) Influence of vertical arching (VA) on lateral pile resistance and (b) Variation of influence of vertical arching with slope angle β ($\phi = 35^o$)

5. Parametric study

As observed analytically in Section 3, the lateral resistance offered by the pile is influenced by parameters such as pile diameter, center-to-center spacing, slope angle and soil's shear strength parameters. A parametric study was conducted to identify the relative significance of individual parameters. A pile-stabilized slope with slope angle, $\beta = 10^o$, was considered. The unit weight of soil was taken as 20 kN/m^3 and slip surface was assumed to intersect the piles at 5 m depth. Fig. 6(a) and 6(b) depict the distribution of lateral resistance from the pile ($D = 0.5$ m) for different spacing-to-diameter ratio (n) for i) $c - \phi$ soil ($\phi = 32^o$ and $c = 20$ kN/m^2) and ii) sand ($\phi = 32^o$, $c =$

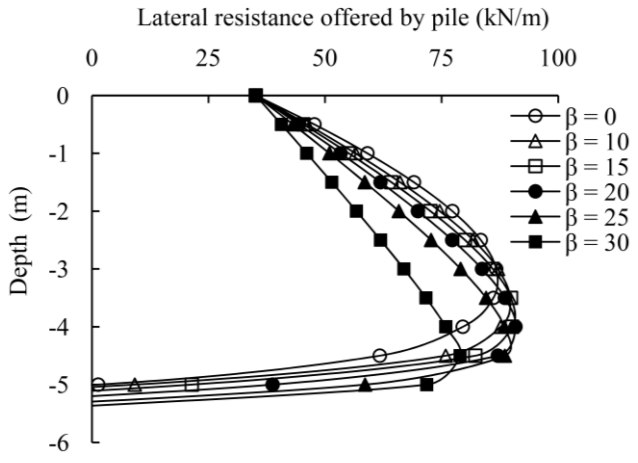

Fig. 10 Distribution of lateral pile resistance for different β

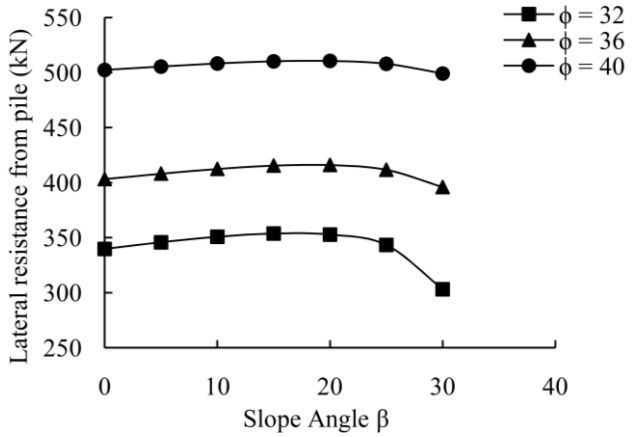

Fig. 11 Resultant lateral pile resistance for different values of ϕ and β

0 kN/m^2) respectively, keeping all other parameters constant. It should be noted that the variation of lateral resistance with depth obtained using the proposed analytical solution is non-linear due to the incorporation of vertical arching; the magnitude of resistance reduces at depth close to slip surface. This causes a shift in the point of action of resultant reaction from the pile. Similar trends in pressure variation were reported by He *et al.* (2015a) as well.

The lateral resistance offered by the pile was found to increase with decrease in the spacing-to-diameter ratio, n (Fig. 6). It can be inferred that, for a given pile diameter, as the center-to-center spacing increases, there is a reduction in arching effect and consequently, the resistance from the pile diminishes. However, no significant reduction in lateral resistance is observed beyond $n = 4$ to 5. Although, arching effect is evident up to a center-to-center spacing of 8D as reported in literature (Liang and Zeng 2002), it is relatively minimal above a spacing of 4 to 5D, which is in accordance with past results (Smethurst and Powrie 2007, Kourkoulis *et al.* 2011b). The influence of diameter on the total lateral resistance offered by the pile is depicted in Fig. 7. As can be observed, for the same s/D ratio, the resultant lateral resistance from the pile increases with increase in diameter. Fig. 8 displays the influence of angle of internal friction on the pile resistance in sand. It is evident from the figure that the soil arching effect is more prevalent in soil with high angle of internal friction.

The non-linearity of lateral resistance is attributed to the presence of vertical arching, and ignoring the same may lead to an overestimation of the pile reaction, especially in frictional soil. The lateral resistance from the pile with and without considering the effect of vertical arching was studied and an example plot is shown in Fig. 9(a). It was observed that an increase of about 25% in resultant lateral resistance from the pile occurred when calculated without considering vertical arching for soil with an angle of internal friction of 35^o and slope angle of 25^o (Fig. 9(a)). In addition, the influence of vertical arching was observed to vary with slope angle β as shown in Fig. 9(b).

Fig. 10 shows the pile resistance distribution for different slope angle β while other parameters are kept constant ($D = 0.5$ m; $n = 3$; $\gamma = 20$ kN/m^3; $c = 20$ kN/m^3; and $\phi = 32^o$). Similarly, Fig. 11 presents the variation of resultant lateral resistance from the pile with slope angle (β) for different angle of internal friction. It is evident from Figs. 10-11 that the pile resistance increases with increase in slope angle up to a certain value (25^o in the present case; Fig. 11) and reduces with further increase in slope angle. The initial increase in the resultant resistance from the pile is due to increase in component of overburden stress along the direction of sliding and as the slope angle (β) approaches the angle of internal friction (ϕ), the stability of slope decreases, thus reducing the total force on the pile.

6. Discussion

In this paper, the pile-stabilized slope is studied considering the soil arching effect both in horizontal and vertical directions and an analytical model is proposed to determine the resistance offered by the pile against slope failure. The presented analytical model is a pressure-based method, which calculates the ultimate lateral pile resistance that can be offered to the deforming soil mass corresponding to an active state of plastic equilibrium between the neighboring piles. The method fairly predicted the lateral force transferred to the piles from the deforming soil mass in case of both sand and $c - \phi$ soil. Note, the scope of the present study was limited to the determination of distribution of the lateral pile resistance, considering the "flow-mode" of pile behavior as demarcated by Poulos (1995). Flow mode of failure generally occurs when the length of the pile within the stable soil layer is relatively deep and therefore, the deformation of sliding mass is larger than the pile deflection (Poulos 1995). The lateral resistance obtained using the proposed method can be subsequently used in the stability analysis of the pile-stabilized slopes and to compute the corresponding factor of safety (Lee *et al.* 1995, Jeong *et al.* 2003, Kourkoulis *et al.* 2011a). The lateral behavior of the pile subjected to the imposed soil thrust, which is necessary for the structural design of the pile, was not investigated. The piles were assumed to be structurally safe against the lateral force due to the soil deformation; in essence, the bending moment and shear force developed in the pile are not incorporated.

7. Conclusions

This paper presents a new analytical method to obtain the lateral resistance offered by stabilizing piles considering the effect of both horizontal and vertical arching for sand and $c-\phi$ soil slopes. The proposed formulation accounts for the influence of various parameters like the pile diameter, center-to-center spacing, slope angle, and shear strength parameters of soil. The point of application of resultant pile resistance can be calculated using this method, incorporating the influence of slope angle. The proposed method was validated using published experimental and numerical results and the method displays a closer agreement when compared to the existing widely used pressure-based methods.

Resultant pile resistance is influenced by the pile diameter and spacing owing to the prevalence of soil arching. The soil arching effect and hence the portion of lateral thrust transferred to the pile are found to increase with increase in the angle of internal friction and decrease with the increase of the pile spacing. Based on the assumptions and the cases examined in this paper, no significant soil arching is visible beyond a pile center-to-center spacing of 4-5D. The resultant pile resistance is seen to initially increase with an increase of slope angle β and then reduces as the slope angle approaches the angle of internal friction of soil.

Acknowledgments

The financial support provided to the first author by the Ministry of Education (MoE), India, for completion of this work is gratefully acknowledged.

References

Adachi, T., Kimura, M. and Tada, S. (1989), "Analysis on the preventive mechanism of landslide stabilizing piles", *Proceedings of the 3rd International Symposium on Numerical Models in Geomechanics*, Niagara Falls, Canada, May.

Ardalan, H. and Mohamed, A. (2013), "Analysis of landslides and slopes stabilized using one row of piles", Research Report No: ATP 4/13/12, Deep Foundation Institute (DFI) and University of Alabama, Huntsville, Alabama, U.S.A.

Ashour, M. and Hamed, A. (2012), "Analysis of pile stabilized slopes based on soil-pile interaction", *Comput. Geotech.*, **39**, 85-97. https://doi.org/10.1016/j.compgeo.2011.09.001.

Ausilio, E., Conte, E. and Dente, G. (2001), "Stability analysis of slopes reinforced with piles", *Comput. Geotech.*, **28**(8), 591-611. https://doi.org/10.1016/S0266-352X(01)00013-1.

Bosscher, P.J. and Gray, D.H. (1986), "Soil arching in sandy slopes", *J. Geotech. Eng.*, **112**(6), 626-645. https://doi.org/10.1061/(ASCE)0733-9410(1986)112:6(626).

Broms, B.B. (1964), "Lateral resistance of piles in cohesive soils", *J. Soil Mech. Found. Div.*, **90**(2), 27-63.

Cai, F. and Keizo, U. (2000), "Numerical analysis of the stability of a slope reinforced with piles", *Soils Found.*, **40**(1), 73-84. https://doi.org/10.3208/sandf.40.73.

Chen, C. and Martin, G.R. (2002), "Soil-structure interaction for landslide stabilizing piles", *Comput. Geotech.*, **29**(5), 363-386. https://doi.org/10.1016/S0266-352X(01)00035-0.

De Beer, E.E. and Wallays, M. (1970), "Stabilization of a slope in schists by means of bored piles reinforced with steel beams", *Proceedings of the International Society of Rock Mechanics*, Lisbon, Portugal, May.

Deng, B. and Yang, M. (2019), "Bearing capacity analysis of pile-stabilized slopes under steady unsaturated flow conditions", *Int. J. Geomech.*, **19**(12), 04019129. https://doi.org/10.1061/(ASCE)GM.1943-5622.0001509.

Di Laora, R., Maiorano, M.S. and Aversa, S. (2017), "Ultimate lateral load of slope-stabilizing piles", *Geotechnique Lett.*, **7**(3), 237-244. https://doi.org/10.1680/jgele.17.00038.

Durrani, I.K., Ellis, E.A. and Reddish, D.J. (2006), "Modelling lateral pile-soil interaction for a row of piles in a frictional soil", *Proceedings of the 4th International FLAC Symposium on Numerical Modelling in Geomechanics*, Madrid, Spain, May.

Ellis, E., Durrani, I.K. and Reddish, D.J. (2010), "Numerical modelling of discrete pile rows for slope stability and generic guidance for design", *Géotechnique*, **60**(3), 185-195. https://doi.org/10.1680/geot.7.00090.

Galli, A. and Di Prisco, C. (2013), "Displacement-based design procedure for slope-stabilizing piles", *Can. Geotech. J.*, **50**(1), 41-53. https://doi.org/10.1139/cgj-2012-0104.

Handy, R.L. (1985), "The arch in soil arching", *J. Geotech. Eng.*, **111**(3), 302-318. https://doi.org/10.1061/(ASCE)0733-9410(1985)111:3(302).

Harrop-Williams, K. (1989), "Arch in soil arching", *J. Geotech. Eng.*, **115**(3), 415-419. https://doi.org/10.1061/(ASCE)0733-9410(1989)115:3(415).

Hassiotis, S., Chameau, J. and Gunaratne, M. (1997), "Design method for stabilization of slopes with piles", *J. Geotech. Geoenviron. Eng.*, **123**(4), 314-323. https://doi.org/10.1061/(ASCE)1090-0241(1997)123:4(314).

He, Y., Hazarika, H., Yasufuku, N., Teng, J., Jiang, Z. and Han, Z. (2015b), "Estimation of lateral force acting on piles to stabilize landslides", *Nat. Hazards*, **79**(3), 1981-2003. https://doi.org/10.1007/s11069-015-1942-0.

He, Y., Hemanta, H., Noriyuki, Y. and Zheng, H. (2015a), "Evaluating the effect of slope angle on the distribution of the soil-pile pressure acting on stabilizing piles in sandy slopes", *Comput. Geotech.*, **69**, 153-165. http://doi.org/10.1016/j.compgeo.2015.05.006.

Hewlett, W.J. and Randolph, M.F. (1988), "Analysis of piled embankments", *Int. J. Rock Mech. Min. Sci. Geomech. Abstr.*, **25**(6), 297-298.

Ho, I.H. (2015), "Numerical study of slope-stabilizing piles in undrained clayey slopes with a weak thin layer", *Int. J. Geomech.*, **15**(5), 06014025. https://doi.org/10.1061/(ASCE)GM.1943-5622.0000445.

Ito, T. and Matsui, T. (1975), "Methods to estimate lateral force acting on stabilizing piles", *Soils Found.*, **15**(4), 43-59. https://doi.org/10.3208/sandf1972.15.4$_4$3.

Ito, T., Matsui, T. and Hong, W.P. (1981), "Design method for stabilizing piles against landslide: One row of piles", *Soils Found.*, **21**(1), 21-37. https://doi.org/10.3208/sandf1972.21.21.

Jaouhar, E.M., Li, L. and Aubertin, M. (2018), "An analytical solution for estimating the stresses in vertical backfilled stopes based on a circular arc distribution", *Geomech. Eng.*, **15**(3), 889-898. https://doi.org/10.12989/gae.2018.15.3.889.

Jeong, S., Kim, B., Won, J. and Lee, J. (2003), "Uncoupled analysis of stabilizing piles in weathered slopes", *Comput. Geotech.*, **30**(8), 671-682. https://doi.org/10.1016/j.compgeo.2003.07.002.

Kellogg, C. and Quinlan, J. (1987), "The arch in soil arching. discussion", *J. Geotech. Eng.*, **113**(3), 269-271. https://doi.org/10.1061/(ASCE)0733-9410(1987)113:3(269).

Khosravi, M., Bahaaddini, M., Kargar, A. and Pipatpongsa, T. (2018), "Soil arching behind retaining walls under active

translation mode: Review and new insights", *Int. J. Min. Geo-Eng.*, **52**(2), 131-140. https://doi.org/10.22059/ijmge.2018.264011.594754.

Kourkoulis, R., Gelagoti, F., Anastasopoulos, I. and Gazetas, G. (2011a), "Hybrid method for analysis and design of slope stabilizing piles", *J. Geotech. Geoenviron. Eng.*, **138**(1), 1-14. https://doi.org/10.1061/(ASCE)GT.1943-5606.0000546.

Kourkoulis, R., Gelagoti, F., Anastasopoulos, I. and Gazetas, G. (2011b), "Slope stabilizing piles and pile-groups: parametric study and design insights", *J. Geotech. Geoenviron. Eng.*, **137**(7), 663-677. https://doi.org/10.1061/(ASCE)GT.1943-5606.0000479.

Lee, C., Hull, T. and Poulos, H. (1995), "Simplified pile-slope stability analysis", *Comput. Geotech.*, **17**(1), 1-16. https://doi.org/10.1016/0266-352X(95)91300-S.

Lee, I.M., Kim, D.H., Kim, K.Y. and Lee, S.W. (2016), "Earth pressure on a vertical shaft considering the arching effect in $c-\phi$ soil", *Geomech. Eng.*, **11**(6), 879-896. https://doi.org/10.12989/gae.2016.11.6.879.

Li, J.P. and Wang, M. (2014), "Simplified method for calculating active earth pressure on rigid retaining walls considering the arching effect under translational mode", *Int. J. Geomech.*, **14**(2), 282-290. https://doi.org/10.1061/(ASCE)GM.1943-5622.0000313.

Li, X. and Wei, S. (2018), "A calculation method for the distribution of lateral force acting on stabilizing piles considering soil arching effect", *Indian Geotech. J.*, **49**(1), 132-139. https://doi.org/10.1007/s40098-018-0307-5.

Liang, R. and Zeng, S. (2002), "Numerical study of soil arching mechanism in drilled shafts for slope stabilization", *Soils Found.*, **42**(2), 83-92. https://doi.org/10.3208/sandf.42.2_3.

Liang, R.Y., Joorabchi, A.E. and Li, L. (2014), "Analysis and design method for slope stabilization using a row of drilled shafts", *J. Geotech. Geoenviron. Eng.*, **140**(5), 04014001. https://doi.org/10.1061/(ASCE)GT.1943-5606.0001070.

Lirer, S. (2012), "Landslide stabilizing piles: Experimental evidences and numerical interpretation", *Eng. Geol.*, **149-150**, 70-77. https://doi.org/10.1016/j.enggeo.2012.08.002.

Moradi, G. and Abbasnejad, A. (2015), "Experimental and numerical investigation of arching effect in sand using modified Mohr Coulomb", *Geomech. Eng.*, **8**(6), 829-844. http://doi.org/10.12989/gae.2015.8.6.829.

Norris, G. (1986), "Theoretically based BEF laterally loaded pile analysis", *Proceedings of the 3rd International Conference on Numerical Methods in Offshore Piling*, Nantes, France, May.

Paik, K. and Salgado, R. (2003), "Estimation of active earth pressure against rigid retaining walls considering arching effects", *Géotechnique*, **53**(7), 643-654. https://doi.org/10.1680/geot.2003.53.7.643.

Poulos, H.G. (1995), "Design of reinforcing piles to increase slope stability", *Can. Geotech. J.*, **32**(5), 808-818. https://doi.org/10.1139/t95-078.

Rao, P., Chen, Q., Zhou, Y., Nimbalkar, S. and Chiaro, G. (2016), "Determination of active earth pressure on rigid retaining wall considering arching effect in cohesive backfill soil", *Int. J. Geomech.*, **16**(3), 04015082. https://doi.org/10.1061/(ASCE)GM.1943-5622.0000589.

Saseendran, R. and Dodagoudar, G. (2020), "Reliability analysis of slopes stabilised with piles using response surface method", *Geomech. Eng.*, **21**(6), 513-525. http://doi.org/10.12989/gae.2020.21.6.513.

Smethurst, J. and Powrie, W. (2007), "Monitoring and analysis of the bending behavior of discrete piles used to stabilise a railway embankment", *Géotechnique*, **57**(8), 663-677. https://doi.org/10.1680/geot.2007.57.8.663.

Song, Y.S., Hong, W.P. and Woo, K.S. (2012), "Behavior and analysis of stabilizing piles installed in a cut slope during heavy rainfall", *Eng. Geol.*, **129-130**, 56-67. https://doi.org/10.1016/j.enggeo.2012.01.012.

Viggiani, C. (1981), "Ultimate lateral load on piles used to stabilize landslides", *Proceedings of the 10th International Conference on Soil Mechanics and Foundation Engineering*, Stockholm, Sweden, June.

Wang, L., Leshchinsky, B., Evans, T.M. and Xie, Y. (2017), "Active and passive arching stresses in $c-\phi$ soils: A sensitivity study using computational limit analysis", *Comput. Geotech.*, **84**, 47-57. https://doi.org/10.1016/j.compgeo.2016.11.016.

Won, J., You, K., Jeong, S. and Kim, S. (2005), "Coupled effects in stability analysis of pile-slope systems", *Comput. Geotech.*, **32**(4), 304-315. https://doi.org/10.1016/j.compgeo.2005.02.006.

GC

Appendix

A: Formulation of vertical average stress $\bar{\sigma}_v$

Referring to Fig. 3(b), the triangle LFF' is in equilibrium state and therefore, it can be ignored in the analysis of vertical equilibrium of the whole differential element (Paik and Salgado 2003, He *et al.* 2015a). The minor principal stress σ_3 acts on plane LF', which can be resolved in vertical direction to obtain σ_{3v} as,

$$\sigma_{3v} = \sigma_3 \frac{\sin\xi \cos\beta}{\cos(\xi+\beta)} \tag{19}$$

Using the principles of origin of planes, it can be proved that

$$\xi = \frac{\pi}{4} + \frac{\phi}{2} - \theta_1;\ \theta = \frac{1}{2}(\phi - \beta + \cos^{-1}\frac{\sin\beta}{\sin\phi})\ ;\text{ and }\ \theta_1 = \frac{1}{2}(\phi + \beta + \cos^{-1}\frac{\sin\beta}{\sin\phi})$$

where, θ is the angle between the slip plane and the slope surface, θ_1, the angle between the slip plane and the horizontal, β, the slope angle and ϕ, the angle of internal friction. Shear stress at face EE' is given by

$$\tau = c + \sigma_h \tan\phi = c + (k_{an}\bar{\sigma}_v + T)\tan\phi \tag{20}$$

Considering the vertical force equilibrium of the differential element dz,

$$\tau dz + (\bar{\sigma}_v + d\bar{\sigma}_v)B' + \sigma_{3v}dz - \bar{\sigma}_v B' - \sigma_h \tan\beta dz - \gamma B' h = 0 \tag{21}$$

where, $B' = (H-z)\cos\theta_1/\sin\theta$ and $h = dz\cos\beta$.

Substituting Eq. (20), Eq. (14), Eq. (19), Eq. (2) and Eq. (13), in Eq. (21) and rearranging,

$$\frac{d\bar{\sigma}_v}{dz} + \bar{\sigma}_v\left(\frac{C_1}{H-z}\right) + \frac{C_2}{H-z} - \gamma\cos\beta = 0 \tag{22}$$

where,

$$C_1 = (K_{an}\tan\phi - K_{an}\tan\beta + m)\frac{\sin\theta}{\cos\theta_1};\ m = \frac{K_{an}}{N\cos^2\theta + \sin^2\theta}\frac{\sin\xi\cos\beta}{\cos(\xi+\beta)} \tag{23}$$

$$C_2 = (T\tan\phi - K_{an}\tan\beta + m)\frac{\sin\theta}{\cos\theta_1};\ t = c + \left(\frac{T + 2c\sin^2\theta/\sqrt{N}}{N\cos^2\theta + \sin^2\theta}\right)\frac{\sin\xi\cos\beta}{\cos(\xi+\beta)} \tag{24}$$

Eq. (22) is in the $dy/dx + Py = Q$ form and can be integrated using method of integration factor to obtain $\bar{\sigma}_v$.

$$\left[\bar{\sigma}_v + \frac{\gamma\cos\beta(H-z)}{1-C_1} + \frac{C_2}{C_1}\right](H-z)^{-C_1} = C \tag{25}$$

where, C is the constant of integration. Applying the boundary condition, $\bar{\sigma}_v = 0$ at $z = 0$, in Eq. (25) gives,

$$C = \left[\frac{\gamma\cos\beta\, H}{1-C_1} + \frac{C_2}{C_1}\right](H)^{-C_1} \tag{26}$$

Substituting for C (Eq. 26) in Eq. 25 and re-arranging,

$$\bar{\sigma}_v = \frac{\gamma\cos\beta\, H}{1-C_1}\left[\left(1-\frac{z}{H}\right)^{C_1} - \left(1-\frac{z}{H}\right)\right] + \frac{C_2}{C_1}\left[\left(1-\frac{z}{H}\right)^{C_1} - 1\right] \tag{27}$$

B: Resultant pile resistance and point of application

The net pile resistance P_r offered by the pile is obtained by integrating Eq. (7) with respect to depth.

$$P_r = \int_0^H \sigma_i(\Lambda+1)D + \frac{2c\sqrt{N}}{N-1}\Lambda D \tag{28}$$

Here, σ_i is a function of z, given by Eq. 14. Substituting Eq. (14) and Eq. (15) in Eq. (28),

$$P_r = \int_0^H \left[\left\{\left\{\frac{\gamma\cos\beta\, H}{1-C_1}\left[\left(1-\frac{z}{H}\right)^{C_1} - \left(1-\frac{z}{H}\right)\right] + \frac{C_2}{C_1}\left[\left(1-\frac{z}{H}\right)^{C_1} - 1\right]\right\}K_{an} + T\right\}(\Lambda+1)D + \frac{2c\sqrt{N}}{N-1}\Lambda D\right]dz \tag{29}$$

Integrating Eq. (29) yields the resultant lateral pile resistance as,

$$P_r = D(\Lambda+1)K_{an}\left[\frac{\gamma\cos\beta\ H^2}{1-C_1}\left(\frac{1}{1+C_1} - \frac{1}{2}\right) + \frac{C_2 H}{C_1}\left(\frac{1}{1+C_1} - 1\right)\right] + TD(\Lambda+1)H + \frac{2c\sqrt{N}\ \Lambda DH}{N-1} \tag{30}$$

The point of application of total lateral resistance is obtained by dividing the moment of this force about point of intersection of the pile with failure surface.

$$M = \int_0^H P(H-z)dz \tag{31}$$

Substituting Eq. (7) in Eq. (31) yields,

$$M = \int_0^H \left[\sigma_i(\Lambda+1)D + \frac{2c\sqrt{N}}{N-1}\Lambda D\right](H-z)dz \tag{32}$$

Substituting Eq. (15) and integrating Eq. (32), gives

$$M = HD(\Lambda+1)K_{an}\left[\frac{\gamma\cos\beta\ H^2}{1-C_1}\left(\frac{1}{1+C_1} - \frac{1}{2}\right) + \frac{C_2 H}{C_1}\left(\frac{1}{1+C_1} - 1\right)\right] - K_{an}D(\Lambda + 1)\left[\frac{\gamma\cos\beta\ H^3}{1-C_1}\left(\frac{1}{(C_1+1)(C_1+2)} - \frac{1}{6}\right) + \frac{C_2 H^2}{C_1}\left(\frac{1}{(C_1+1)(C_1+2)} - \frac{1}{2}\right)\right] + TD(\Lambda+1)\frac{H^2}{2} + \frac{2c\sqrt{N}\ \Lambda DH^2}{(N-1)2} \tag{33}$$

Eqs. (33) and (30) can be used to obtain the point of action as,

$$H_r = \frac{M}{P_r} \tag{34}$$